

Collective dynamics of logic active particles

Matteo Paoluzzi^{1,2,*}, Marco Leoni^{3,†} and M. Cristina Marchetti⁴

¹ *ISC-CNR, Institute for Complex Systems, Piazzale A. Moro 2, I-00185 Rome, Italy*

² *Dipartimento di Fisica, Sapienza University of Rome, Piazzale A. Moro 2, I-00185, Rome, Italy*

³ *Université Paris-Saclay, CNRS, Laboratoire de l'accélérateur linéaire, 91898, Orsay, France*

⁴ *Department of Physics, University of California Santa Barbara, Santa Barbara, CA 93106, USA*

(Dated: December 31, 2023)

We examine the interplay of motility and information exchange in a model of run-and-tumble active particles where the particle's motility is encoded as a bit of information that can be exchanged upon contact according to the rules of AND and OR logic gates in a circuit. Motile AND particles become non-motile upon contact with a non-motile particle. Conversely, motile OR particles remain motile upon collision with their non-motile counterparts. AND particles that have become non-motile additionally recover their motility or “reawaken” at a fixed rate μ , as in the SIS (Susceptible, Infected, Susceptible) model of epidemic spreading, where an infected agent can become healthy again, but keeps no memory of the recent infection, hence it is susceptible to a renewed infection. For $\mu = 0$, both AND and OR particles relax irreversibly to absorbing states of all non-motile or all motile particles, respectively, although the relaxation kinetics is faster for OR particles that remain active throughout the process. At finite μ , the AND dynamics is controlled by the interplay between reawakening and collision rates. The system evolves to a state of all motile particles (an absorbing state in the language of absorbing phase transitions) for $\mu > \mu_c$ and to a mixed state with coexisting motile and non-motile particles (an active state in the language of absorbing phase transitions) for $\mu < \mu_c$. The final state exhibits a rich structure controlled by motility-induced aggregation. Our work can be relevant to biochemical signaling in motile bacteria, the spreading of epidemics and social consensus, as well as light-controlled organization of active colloids.

I. INTRODUCTION

Swimming bacteria and living cells are examples of entities that consume energy to generate autonomous motion. Through interactions, these systems organize in complex patterns on scales much larger than those of the individual constituents. This behavior has provided inspiration for the development of the field of active matter that has had remarkable success at describing some of the spontaneous organization seen in nature on many scales, from the flocking of birds to the collective migration of epithelial cells in wound healing [1–4].

So far most active matter studies have focused on the role of reciprocal mechanical or rule-based interactions, such as steric repulsion or medium-mediated hydrodynamic couplings, in controlling the emergence of nonequilibrium collective behavior. But living entities often interact through the exchange of information transmitted through biochemical signaling, chemical, visual and other clues. Information exchange carried by motile individuals is often non-reciprocal and its role in controlling emergent structures in collections of motile agents is only beginning to be explored [5–11].

An example of information exchange common in nature is biochemical signaling that controls communication among microbes [12, 13] and chemotaxis [14, 15], driving the formation of complex patterns [16]. This has been modeled extensively by coupling a diffusive agent

to continuum models of active gels [17] and agent-based simulation [18]. Closer in spirit of the model considered here is recent experimental work on active colloids where activity can be controlled by an external feedback loop that tunes the light intensity responsible for driving the colloids' motility [19, 20], mimicking the use of light intensity to control and trigger collective behaviors in photokinetic bacteria [21, 22]. More sophisticated examples include light-activated colloidal particles able to *learn* and to share information with other particles while interacting with the external environment [23]. Finally, information exchange among motile individuals is directly relevant to the understanding of epidemic spreading, social dynamics and robotic communication [8, 24–27].

Much quantitative understanding of the behavior of active systems has come from the minimal model of Active Brownian or Run-and-Tumble Particles (ABP or RTP) consisting of collections of self-propelled spherical particle with purely repulsive interactions that propel themselves at fixed speed and change direction through rotational noise or tumbling events. Building on this body of work, we recently considered a minimal model of active agents where the particle's motility is encoded as a bit of information that can be exchanged upon contact interaction [28] according to logic rules corresponding to AND and OR gates in an electronic circuit. Motile particles obeying AND rules always lose their motility upon interactions with non-motile ones. In this case an initial state of one non-motile particle in a sea of motile ones always evolves to an absorbing state where all particles are nonmotile. Conversely, OR motile particles remain motile when interacting with nonmotile ones. In this case an initial state of one motile particle in a sea

*Electronic address: mtpaoluzzi@gmail.com

†Electronic address: leoni@lal.in2p3.fr

of non-motile ones always evolves towards the symmetric absorbing state where all particles are motile. This model is analogous to SI models (S, susceptible, I, infected) of epidemic spreading where information is transmitted only in one direction and irreversibly, with motile particles corresponding to healthy agents and non-motile particles to infected ones.

In the present paper we examine a richer model analogue to SIS (Susceptible, Infected, Susceptible) models of epidemic spreading [29], where an infected agent can become healthy again, but keeps no memory of the recent infection, hence it is susceptible to a renewed infection [10]. We do this by allowing non-motile particles to regain their motility or “re-awaken” at an average rate μ . The dynamics is then controlled by the interplay between reawakening rate and collision rate, with a critical value μ_c of reawakening rate controlling the properties of the final steady state. For $\mu \geq \mu_c$ the system reaches an absorbing state where all particles are motile. In the terminology of absorbing state phase transitions, this state, although composed entirely of motile particles, is *inactive* because the spreading of nonmotile particles has ceased [30, 31]. For $0 < \mu < \mu_c$ we have a mixed state of motile and nonmotile particles. Again, in the language of absorbing states, this is an *active* state because it is a dynamical steady state where particles continue to exchange their motility. To avoid confusion, we will refer to these two states as *motile* and *mixed*, respectively. For $\mu = 0$ the system evolves at long times to the absorbing state where all particles are non-motile. Our simulation suggests that this state only exists for $\mu = 0$, and that the system remains mixed for any finite value of $\mu < \mu_c$. This could, however, be a consequence of the unavoidable finite time scale of our simulations. Whether there is a lower, but finite critical value of μ below which the system reaches the absorbing non-motile state remains an open question.

A pictorial phase diagram depicting snapshots of representative steady-state configurations is shown in Fig. 1. Both motile and mixed states show a rich spatial organization. In the motile state at $\mu \geq \mu_c$, motile particles exhibit motility-induced phase separation (MIPS) [32–34] at high density and low tumbling rates. In the mixed state, we find spatial patterns at both low and high total density. At low densities nonmotile particles form a cluster surrounded by a gas of motile particles. At high densities the interplay between aggregation of non-motile particles and MIPS results in the opening of bubbles in a mixed background in what resembles a reverse MIPS, as observed in single components ABPs at very high density and motility [34–36]. This effect is most pronounced at low tumbling rates, where the dynamics is most persistent, suggesting that it is indeed driven by motility.

Our work shows that the interplay of motility and information spreading is responsible for complex spatial structures that can be controlled by tuning the total particle density and the re-awakening rate. This suggests that our model may be relevant to recent experimental

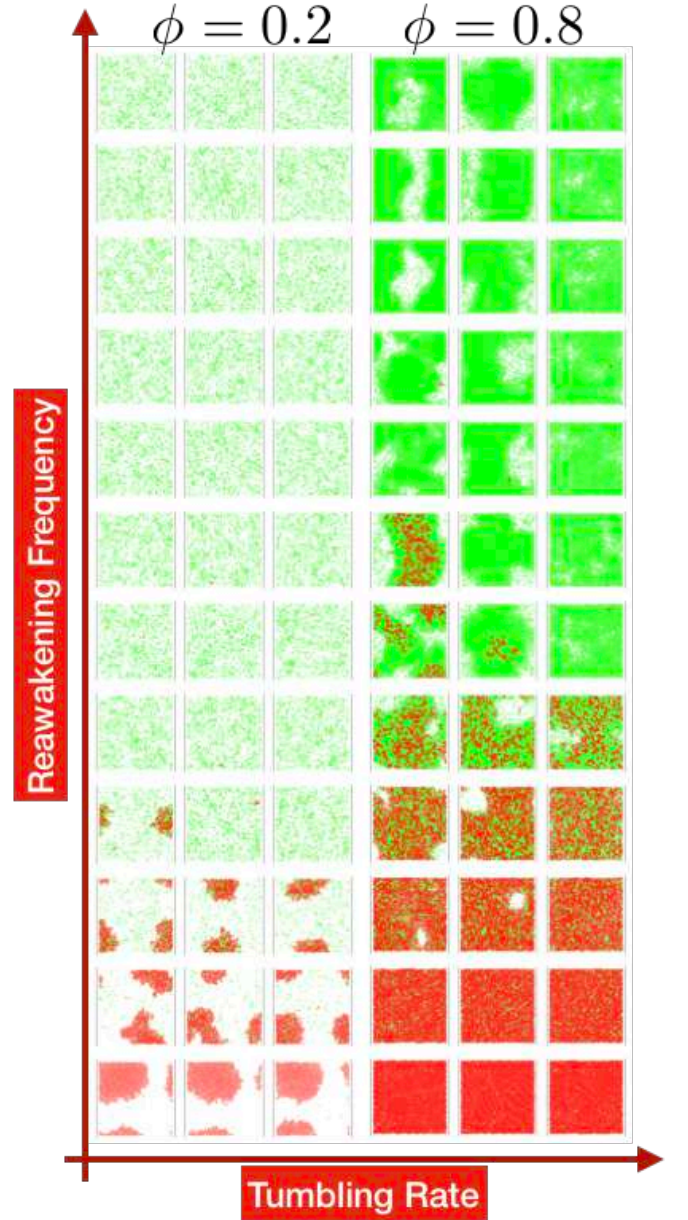


FIG. 1: Representative snapshots of the final configuration of AND particles for two values of the total packing fraction ϕ , $\phi = 0.2$ (left) and $\phi = 0.8$ (right). Red particles are non-motile, green particles are motile. The tumbling rate is $\lambda = 0.01, 0.1, 1$ from left to right at each packing fraction. At both packing fractions the system escapes the absorbing state as the awakening rate is increased. At low packing fraction, the mixed state separates into a cluster on non-motile particles surrounded by a gas of motile ones. At high packing fraction, motile particles in the active state exhibit MIPS, while the mixed state is homogeneous.

work on engineered active particles where the motility of individual particles can be controlled optically. It also provides a new approach to problems such as epidemics or opinion spreading [27, 37, 38]. While these problems have been studied extensively, most previous

work has been carried out for agents sitting on a network of fixed connectivity [39, 40]. In our model, in contrast, the connectivity changes in time as it is determined by the agent dynamics, and the properties of such dynamics affect information spreading. Finally, the model could be adapted to describe the exchange of other internal traits other than motility. In certain bacteria or eukaryotic cells contact interactions are in fact needed for the exchange of chemical signaling, as is the case for instance for C-signaling that mediates collective motility in the bacteria *Myxococcus Xanthus*.

The details of the agent-based model are introduced in Section II, where we also describe a mean-field logistic-type model that reproduces the relaxation to the steady state at low and high density, but fails at intermediate density. In Section III we present the results of the numerical simulations at both $\mu = 0$ (section III.A) and finite μ (section III.B). One new result shown in Section III.A is that in spite of the apparent symmetry of the rules for information transmission upon the exchange of motile into nonmotile particles (see Table I below) when $\mu = 0$ the relaxation to the absorbing state is considerably faster for OR particles than that of AND particles as a result of the active dynamics. In Section III.B we present the metrics used to construct quantitative phase diagrams and to characterize the relaxation kinetics and the structure of the steady states. In Section IV we discuss a continuum model (with some details in Appendix A) and conclude with a few remarks in Section V.

II. MODEL

We consider N spherical particles of diameter a performing run-and-tumble dynamics in two dimensions. The particles have identical size, self propulsion velocity, and tumbling rate. Moreover, they interact via short-range repulsive interactions. They are only distinguished by their motility state (motile or non-motile) represented by their color (green for motile and red for non-motile). Particles exchange their motility state upon collision according to rules inspired by logic gates. The motility state of AND particles evolves according to the rules associated with the AND gate of a logic circuit that gives a high output only if all its inputs are high. Conversely, OR particles evolve according to the rules associated with an OR gate that gives a high output if one or more of its inputs are high. The corresponding interaction rules are given in Table I. In Fig. (1) and throughout the paper, we represent nonmotile particles as red (R) and motile particles as green (G).

In the case of AND rules, non-motile (red) particles can also re-acquire their motility, or “reawaken”, at a rate μ . When $\mu = 0$ the loss/gain of motility is analogue to the spreading of disease in the Susceptible-Infected (SI) model of epidemics dynamics, with motile particles corresponding to infected individuals and black to susceptible individuals. For finite values of μ the model

AND	OR
$G + R \rightarrow R + R$	$G + R \rightarrow G + G$
$R + G \rightarrow R + R$	$R + G \rightarrow G + G$
$G + G \rightarrow G + G$	$G + G \rightarrow G + G$
$R + R \rightarrow R + R$	$R + R \rightarrow R + R$

TABLE I: The logic interaction rules that control motility exchange among non-motile/red (R) and motile/green (G) particles interacting via AND and OR rules.

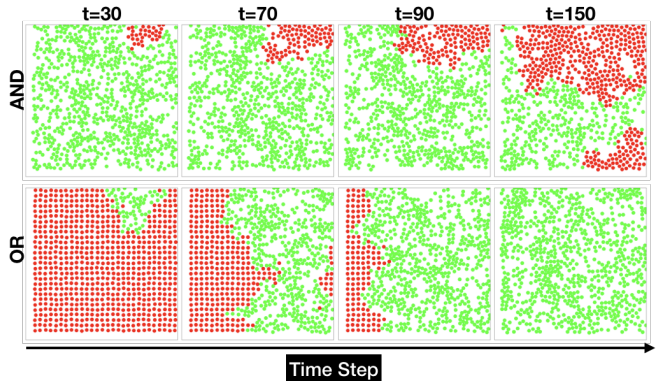


FIG. 2: Snapshots of the approach to the absorbing state for AND (top row) and OR (bottom row) particles at $\phi = 0.55$, $\lambda = 1$ and $\mu = 0$. Motile particles are green and non-motile particles are red. The snapshots for AND and OR particles are taken at the same time steps $t = 30, 70, 90, 150$, as indicated.

corresponds to the Susceptible-Infected-Susceptible (SIS) model of epidemics spreading [29].

a. Agent-based model. Denoting the motility state of particle i by an internal variable $\sigma_i(t)$, with $\sigma = 0, 1$ for non-motile and motile particles, respectively, the dynamics of the system is described by the equations

$$\mathbf{v}_i = v_0 \mathbf{e}_i \sigma_i (1 - s_i) + \xi \sum_{i \neq j} \mathbf{f}(r_{ij}), \quad (1)$$

$$\boldsymbol{\omega}_i = \mathbf{t}_i^r s_i \sigma_i, \quad (2)$$

where $\mathbf{v}_i = \partial_t \mathbf{r}_i$ and $\boldsymbol{\omega}_i = \mathbf{e}_i \times \partial_t \mathbf{e}_i$ are the translational and angular velocity of a particle at positions \mathbf{r}_i . The orientation \mathbf{e}_i specifies the direction or motion during the run phase. The first term on the right hand side of Eq. (1) describes propulsion at speed v_0 , with s_i an auxiliary state variable that is 0 during the run and 1 in the tumble state. Details about the model can be found in [41, 42]. During the tumbling state, particle i receives a random torque \mathbf{t}_i^r that rotates the direction of its orientation \mathbf{e}_i . Tumbles are Poisson-distributed with mean rate λ . The second term on the right hand side of Eq. (1) describes repulsive interactions, with $\mathbf{f}(r_{ij}) = -\nabla_i V(r_{ij})$ and $V(r) = \frac{\epsilon}{12} (\frac{a}{r})^{12}$ the interaction potential among two particles at separation $r_{ij} = |\mathbf{r}_i - \mathbf{r}_j|$, ϵ the energy scale and ξ the mobility. We choose $\epsilon = 1$ in all the following. For the case of overdamped dynamics considered here, particles exchange momentum instantaneously upon col-

lision. Hence, collisions do not lead to rearrangement of non-motile particles.

b. Mean-field model. Before discussing the numerical results it is useful to formulate a simple mean-field model in terms of the number densities ρ_G and ρ_R of motile (green) and non-motile (red) particles. We will formulate the mean-field model for the case of particles interacting with AND rules, where reawakening is important. Neglecting all spatial variations, the mean field dynamics of AND particles is governed by

$$\partial_t \rho_G = -\beta \rho_G \rho_R + \mu \rho_R, \quad (3)$$

$$\partial_t \rho_R = \beta \rho_G \rho_R - \mu \rho_R, \quad (4)$$

where β is a parameter with dimensions of inverse time/density that controls the rate of collisions. The case of OR particles can be obtained from the above by setting $\mu = 0$ and interchanging motile and nonmotile particles. The total density $\rho = \rho_G + \rho_R$ is constant, with $\rho = \rho_0$ and the coupled equations can be recast in the form of a single equation for the fraction $m = \rho_G/\rho$ of motile particles, given by

$$\partial_t m = -\beta \rho_0 m(1-m) + \mu(1-m). \quad (5)$$

The homogeneous steady states are controlled by the interplay between the time $\tau = (\beta \rho_0)^{-1}$ at which collisions turn motile particles into non-motile ones and the reawakening rate μ . One finds two stable states: an absorbing state of all motile particles ($m^* = 1$) when $\mu\tau > 1$ and a mixed state with a fraction $m^* = \mu\tau$ of motile particles for $\mu\tau < 1$. In the absence of reawakening ($\mu = 0$) the mixed state is an absorbing state where all particles are non-motile. We will see below that fluctuations not captured by the simple logistic model (modified by reawakening) given in Eq. (5) can yield a rich structure for both the absorbing and mixed states.

The mean-field model can be solved exactly to obtain the kinetics of approach to the steady state, with the result

$$m(t) = \frac{m_0 - \mu\tau - \mu\tau(m_0 - 1)e^{(1-\mu\tau)t/\tau}}{m_0 - \mu\tau - (m_0 - 1)e^{(1-\mu\tau)t/\tau}} \quad (6)$$

for a given initial fraction $m_0 = m(t=0)$ of motile particles. Clearly $m(t)$ relaxes to $m^* = 1$ for $\mu\tau > 1$ and to $m^* = \mu\tau$ for $\mu\tau$ for all initial values m_0 , other than of course $m_0 = 1, \mu\tau$. The kinetics of approach to the steady states is controlled by the shortest of the collision and reawakening times, and the dynamics can become very slow near the critical line separating the two steady states, where these two time scales are comparable.

III. NUMERICAL RESULTS

We have simulated the dynamics of N particles in a square box of side L , with periodic boundary conditions. We have varied the packing fraction $\phi = NA_s/L^2 \equiv \rho A_s$,

with $A_s = \pi(a/2)^2$, by varying the number of particles N at fixed L . We have solved numerically Eqs. (1),(2) using a second order Runge-Kutta scheme with time step $dt = 10^{-3}$ and $\mu = v_0 = 1$. The results presented below have been obtained considering $L = 80a$ and varying ϕ in the range $[1 \cdot 10^{-2} \div 0.79]$ for $\lambda = 0.01, 0.05, 0.1, 0.5, 1, 5$.

All simulations are initiated with one G particle in a sea of R particles for AND rules and conversely with one R particle in a sea of G particles for OR rules.

A. No reawakening and absorbing states

We first examine the results of the model with $\mu = 0$. Clearly in this case for both AND and OR rules the system evolves irreversibly towards an absorbing state with all red (AND) or all green (OR) particles. Snapshots of the time evolution towards the absorbing state are shown in Fig. 2 for AND (top row) and OR (bottom row) particles at the same total packing fraction. Snapshots in the same column are taken at the same time instant and show that the approach to the absorbing state is faster for OR particles. It is clear from the rules given in Table I that if the particles were to only exchange their color upon collision, while retaining their motile state, the two sets of rules would be symmetric when interchanging green and red. In this case the relaxation of AND and OR particles will be identical. Exchanging motility removes this symmetry and affects the dynamics.

To quantify the relaxation kinetics, we measure the fraction $m(t)$ of motile particles, with $m(t) = N^{-1} \sum_i \sigma_i(t)$. The evolution of $1 - m(t)$ for OR particles is shown in Fig. 3(top panel) for different densities. At low and high density the dynamics is well reproduced by the logistic model given in Eq. (6) with $\mu = 0$ shown as dashed lines. The logistic model fails, however, at intermediate densities. The evolution of $m(t)$ for AND particles was shown in Ref. [28]. The fact that the logistic model does not fit the data at intermediate densities indicates that in this regime the relaxation dynamics cannot be described by a single time scale. The existence of a distribution of relaxation time is highlighted by the dynamical susceptibility $\chi(t)$ defined as $\chi(t) = \langle (m(t) - \langle m(t) \rangle_s)^2 \rangle_s$, where $\langle \dots \rangle_s = \dots$ denotes the average over 50 realizations. This quantity measures sample-to-sample fluctuations in the time-evolution of $m(t)$. It is analogous to, but distinct from, the 4-point susceptibility used in glassy physics that measures sample-to-sample fluctuations of the overlap between configurations accessed by the system at different times. The susceptibility, shown in Fig. 3, bottom panel, displays a sharp peak at both low and high packing fraction ϕ , suggesting that the kinetics of approach to the absorbing state is controlled by a single relaxation time which is distinctly shorter for OR particles. At intermediate density, in contrast, fluctuations are broad, indicating that the dynamics is governed by a distribu-

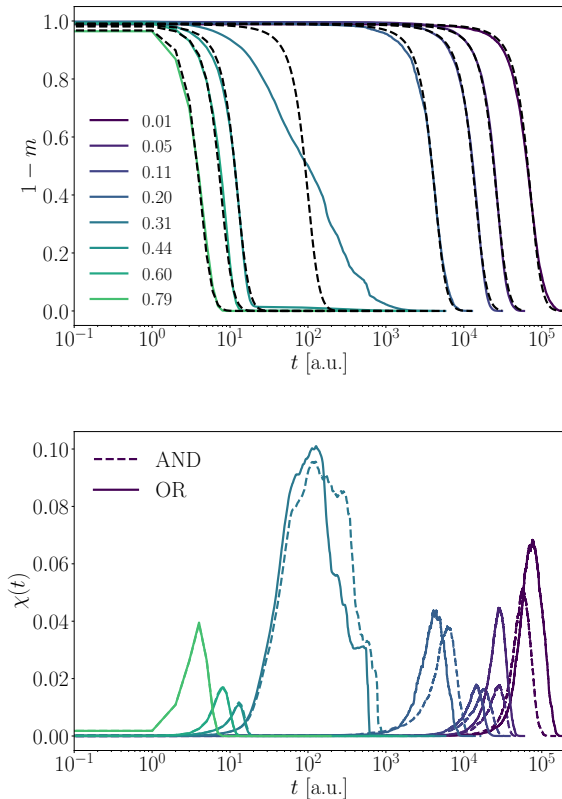


FIG. 3: Top: fraction $1 - m(t)$ of motile OR particles as a function of time for various values of the packing fraction ϕ . The curves through the data are fits to the logistic form, Eq. (6). Bottom: Susceptibility $\chi(t)$ as a function of time (in arbitrary units) obtained from sample-to-sample fluctuations for AND (dashed) and OR (solid) particles. The different curves are for the same values of packing fraction used in the top panel. Both figures are for $\lambda = 1$ and $\mu = 0$.

tion of relaxation times. We note that the complex kinetics obtained at intermediate density is not associated with the coupling between AND/OR rules and motility, but it also occurs for particles that only exchange color upon collision, while remaining always motile. The broad distribution of relaxation times arises instead from the anomalous density fluctuations that are a signature of active systems.

Finally, we extract a mean relaxation time $\tau_m = \langle \hat{\tau} \rangle_s$, where $\hat{\tau}$ is defined by $m(\hat{\tau}) = 0$ for AND particles and $m(\hat{\tau}) = 1$ for OR particles. The mean time τ_m is shown in Fig. 4 as a function of the total packing fraction. The plot clearly shows the faster relaxation of OR particles at low packing fraction. At high packing fraction, the curves are essentially on top of each other, and also agree with the relaxation for the case when motility and particle color are decoupled and all particles retain their motility upon collision. The difference in the relaxation of OR and AND particles when the internal state is coupled to motility can be easily understood by noting that for AND

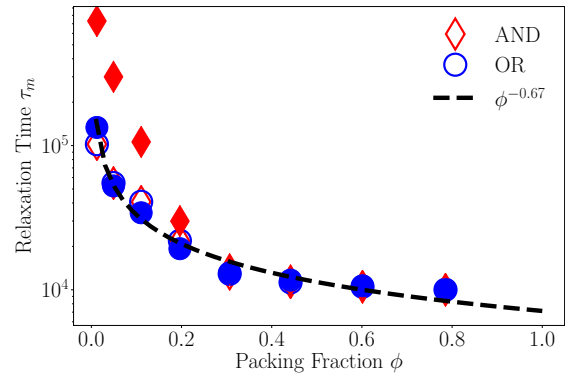


FIG. 4: Relaxation time, τ_m , as a function of packing fraction. Red diamonds refer to AND particles, blue circles to OR particles. Filled symbols correspond to the case where particles change their motility state upon collision according to the logic rules of Table I. Open symbols are for the case where particles only exchange their color upon collisions, but always retain their motility. When the internal state and motility are decoupled the relaxation to the steady state is the same for AND and OR rules. When motility is exchanged according to the logic rules, OR particles relax faster than AND ones. The black dashed line is a fit to $\tau_m \sim \phi^{-0.67}$.

rules the density of non-motile particles grows at a rate $\sim \beta \rho_0$ controlled entirely by collisions with other particles. In contrast, for OR rules motile particles can additionally diffuse due to their motility, hence density variations over a region ℓ grow at a higher rate $\sim \beta \rho_0 + \frac{v_0^2}{\lambda \ell^2}$. When interactions only result in color exchange, while particles remain always motile, then all particles diffuse and the relaxation rates become identical, as shown in Fig. 4.

B. Reawakening: mixed state and MIPS

We now consider the case when μ is finite, which allows non-motile particle to become motile again, or *reawaken*, at an average rate μ .

We have studied numerically AND particles at two values of the total packing fraction: (i) high packing fraction ($\phi = 0.8$), where one expects that the relaxation towards the steady state may be captured by a mean-field description, and (ii) intermediate packing fraction ($\phi = 0.2$), where local density fluctuations become important. We have constructed a phase diagram by varying the tumbling rate λ and the reawakening rate μ , at fixed self-propulsion velocity v . Working at fixed density ensures that the reaction rate β varies only due to changes in the tumbling rate, allowing us to quantify the importance of density fluctuations due to self-propulsion on the phase transition to the absorbing state. The phase diagrams for $\phi = 0.2, 0.8$ have been obtained for $\lambda \in [0.01, 5]$ and $\mu \in [10^{-4}, 10^{-1}]$.

Because of reawakening, the fraction of motile particles

$m(t)$ fluctuates in time in the steady-state. To characterize then mean behavior, we then define the time-average of the dynamical observable $\mathcal{O}(t)$ over a time T as

$$\langle \mathcal{O}(t) \rangle \equiv \frac{1}{T} \int_{t_0}^{t_0+T} dt \mathcal{O}(t). \quad (7)$$

where t_0 is chosen large enough to guarantee that we have reached the steady-state, and $T \gg t_0$.

For finite μ , as found from the logistic model, the behavior is controlled by the interplay of reawakening and collisions. Starting with one motile (G) particle in a sea on non-motile (R) particles, AND particles relax to one of two states: (i) an absorbing state of all motile particles with $\langle m(t) \rangle = m_A = 1$ for $\mu > \mu_c$, referred to as *motile state*, and, (ii) a *mixed state* with $\langle m(t) \rangle = m_M < 1$ and a finite fraction of non-motile particles for $\mu < \mu_c$. This behavior is evident in the relaxation of $m(t)$ shown in Fig. (5) for $\phi = 0.2$ (left) and $\phi = 0.8$ (right). The absorbing state of all non-motile particles ($m_M = 0$) is obtained here only for $\mu = 0$. The structural and dynamical properties of this state were studied in Ref. [28]. The behavior of m_M is shown in Fig. (6) as a function of μ for the two representative packing fractions. The dashed red lines in Fig. 5 are fits to the analytical mean field solution given in Eq. (6), where μ and τ are two fitting parameters. The mean-field model fits well at high packing fraction (right column, $\phi = 0.8$), but fails at low packing fraction when density fluctuations are important (left column, $\phi = 0.2$).

The steady state behavior is summarized in the pictorial phase diagram shown in Fig. 1 that displays typical snapshots of the long-time configurations. The snapshots show a clear propensity of particles to aggregate. The aggregation of motile green particles at high density is a manifestation of motility-induced phase separation (MIPS) that is most pronounced at low tumbling rate, when the single-particle dynamics is persistent. At $\phi = 0.2$ no MIPS is expected in the range of parameters considered here. Snapshots of the absorbing state at low reawakening for $\phi = 0.2$ show a different type of aggregation, corresponding to phase separation between green and red particles, with a compact cluster of non-motile red particles surrounded by a gas of motile green particles.

To quantify the transition between motile and mixed states, we have examined the steady-state susceptibility χ_s defined as $\chi_s = \langle (\langle m_s(t) \rangle - \langle m_s \rangle_s)^2 \rangle_s$, where $\langle \dots \rangle_s$ denotes a sample average. The susceptibility χ_s is a measure of sample-to-sample fluctuations of the order parameter $\langle m \rangle$. χ_s and it is shown in Fig. (7) as a function of μ for different values of λ . We identify μ_c with the location of the peak in the susceptibility. At intermediate density the location of the peak shift to lower values of μ with increasing tumbling rate, while at high density it is essentially independent of tumbling rate.

To quantify the structural properties of the steady state, we have evaluated the probability distribution

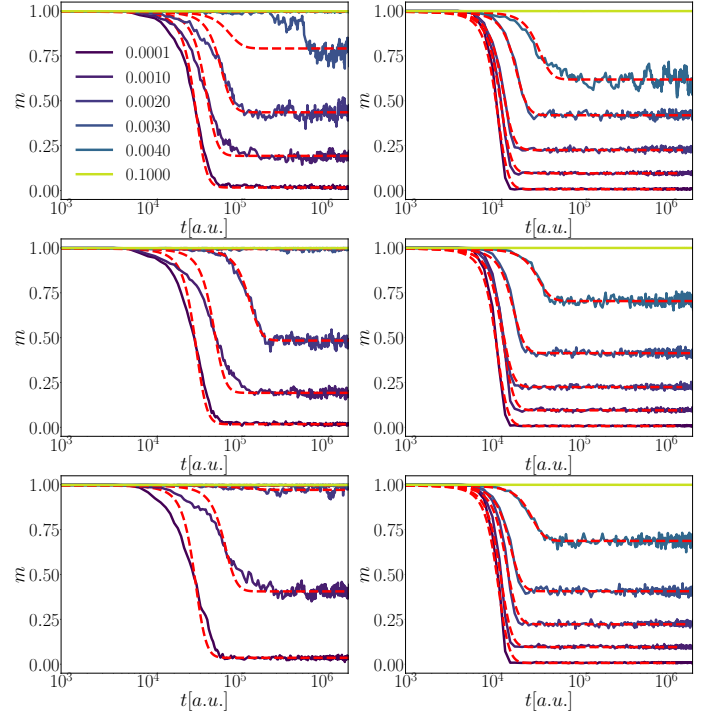


FIG. 5: Time evolution of $m(t)$ as the reawakening frequency increases ($\mu = 10^{-4}, 10^{-3}, 2 \times 10^{-3}, 3 \times 10^{-3}, 4 \times 10^{-3}, 10^{-1}$, from violet to yellow) from green to violet, respectively), for $\phi = 0.2$ (left column) and $\phi = 0.8$ (right column) at different values of λ : $\lambda = 0.01$ (top row), $\lambda = 0.1$ (middle row) and $\lambda = 1$ (bottom row). Dashed red lines are fits to the mean-field model.

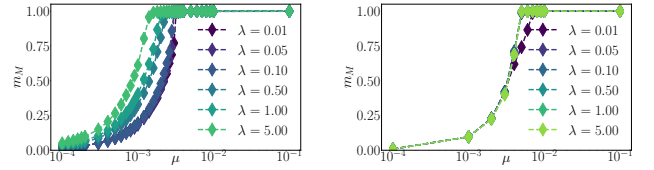


FIG. 6: The order parameter m_M as a function of μ for $\phi = 0.2$ (left) and $\phi = 0.8$ (right).

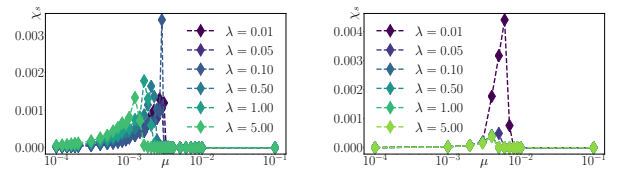


FIG. 7: Steady-state susceptibility χ_s as a function of μ for $\phi = 0.2$ (left) and $\phi = 0.8$ (right). The position of the peak depends on λ for $\phi = 0.2$, while it is essentially independent of λ for $\phi = 0.8$.

$P(\hat{\phi})$ of local packing fractions $\hat{\phi}$ evaluated by discretizing the position of particles on a lattice of linear size $\ell = 4a$. The behavior of $P(\hat{\phi})$ with reawakening rate

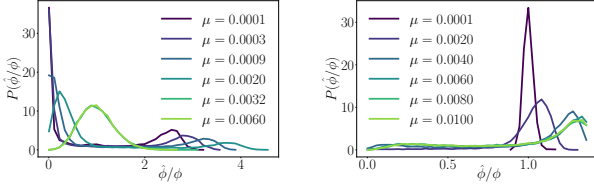


FIG. 8: Probability distribution function of density fields for $\phi = 0.2$ (left) and $\phi = 0.8$ (right) and $\lambda = 0.01$.

μ is shown in Fig. (8) for $\phi = 0.2$ (top) and $\phi = 0.8$ (bottom) for $\lambda = 0.01$. Both plots show an evolution from a unimodal distribution corresponding to a homogeneous state to a bimodal distributions corresponding to a phase separated state, but the mechanisms driving phase separations are distinct at intermediate and high density. For $\phi = 0.2$ one observes phase separation between motile and non-motile particles in the asymptotic mixed state. This phase separation is driven by reaction-diffusion and weakly affected by μ . For $\phi = 0.8$ we find MIPS of motile particles in the absorbing state, hence the phase separation is driven by motility.

The resulting phase diagrams are shown in Fig. (9) for $\phi = 0.2$ (top) and $\phi = 0.8$ (bottom). The blue symbols correspond to the peak in χ_s . The black symbols have been obtained by calculating the Binder cumulant g_4 of the distribution of local density $P(\hat{\phi})$ defined as $g_4 = 1 - \langle \hat{\phi}^4 \rangle / 3 \langle \hat{\phi}^2 \rangle^2$ [43–45]. A negative peak in g_4 corresponds to a bimodal $P(\hat{\phi})$, signaling a first-order phase transition [46]. The color indicates the long-time value of m , with green corresponding to $m = 1$ and red to $m = 0$.

At intermediate densities, the active state for $\mu > \mu_c$ does not undergo MIPS for the range of motility parameters explored here. The mixed state at $\mu < \mu_c$ is always clustered, and the emerging of the structural patterns is due solely to the reaction-diffusion dynamics. In contrast to the prediction of the mean-field model, the transition line $\mu = \mu_c$ does not depend on λ . In particular, as λ decreases and thus motility becomes more persistent, μ_c increases slightly. This finding indicates that the spreading of an internal state in a system of active agents is faster than in the case of Brownian walkers.

At high densities density fluctuations are suppressed and the transition line at $\mu = \mu_c$ is essentially independent of λ , confirming that the mean-field model becomes provide a good description of the system. In contrast to what observed for $\phi = 0.2$, the absorbing state is highly homogeneous, as evident from the snapshots in Fig. (1). In the active state, however, motile particles undergo MIPS [32–34]. We note that at low λ , when the dynamics of active particles is most persistent, MIPS actually occurs even in the mixed phase, provided the fraction of motile particles is sufficiently large. For a fixed tumble rate λ , reawakening tends to suppress MIPS.

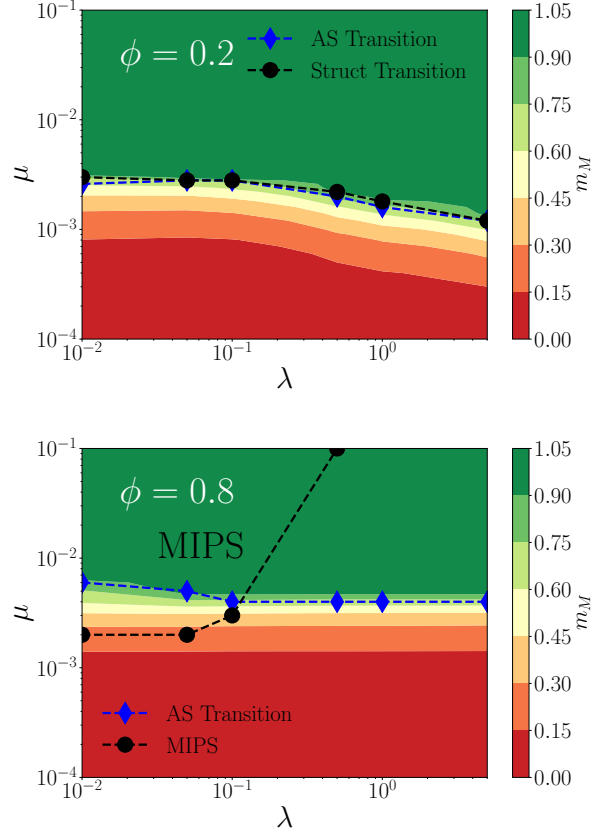


FIG. 9: Phase diagram for $\phi = 0.2$ (top) and $\phi = 0.8$ (bottom) in the λ vs μ plane. The blue diamonds correspond to the transition between mixed and active states identified with the location of the peak in the susceptibility χ_s . The black circles are the points where the Binder cumulant $g_4(\lambda, \mu)$ becomes negative, signaling the onset of separated phases. The color shows to the value of m , with red corresponding to $m = 0$ and green to $m = 1$.

IV. CONTINUUM MODEL

To go beyond the mean-field model discussed in section II, we construct a continuum model that incorporates the current of motile particles. Considering particles interacting with AND rules and including re-awakening, the continuum equations are written as [35, 47]

$$\partial_t \rho_R = \beta \rho_G \rho_R - \mu \rho_R, \quad (8)$$

$$\partial_t \rho_G = -\beta \rho_R \rho_G + \mu \rho_R - \nabla \cdot [v(\rho_G) \mathbf{J}], \quad (9)$$

$$\partial_t \mathbf{J}(\mathbf{r}, t) = -\lambda_{eff} \mathbf{J} - \frac{1}{2} \nabla [v(\rho_G) \rho_G] - \nabla \kappa \nabla^2 \rho_G, \quad (10)$$

where \mathbf{J} is the current density of motile particles and $v(\rho_G)$ is the propulsive speed of motile particles suppressed by crowding as in models of MIPS. We use the simple form

$$v(\rho_G) = v_0 \left(1 - \frac{\rho_G}{\rho^*} \right), \quad \rho_G \leq \rho^* \quad (11)$$

and $v(\rho_G) = 0$ for $\rho_G > \rho^*$, where ρ^* is a characteristic density that depends on particle motility and tumbling rate. It was estimated via kinetic arguments for instance in Ref. [35]. In our model non-motile particles are truly static and do not diffuse, and we neglect small cross-diffusion terms [47]. Collisions instantaneously change the state of a particle from motile to non-motile and are incorporated in the reaction term proportional to β , hence do not contribute to suppression of the propulsive speed. On the other hand, the reaction term $\sim \beta$ renormalizes the tumbling rate of the motile agents to an effective tumbling rate $\lambda_{eff} = \lambda + \beta\rho_R$. We also neglect small cross-diffusion terms in the dynamics of motile particles. Finally, the last term on the right hand side of Eq. (10) represents a phenomenological surface tension $\kappa > 0$ that controls gradients in the density of motile particles.

On time scales long compared to λ_{eff} , we can neglect the left hand side of Eq. (10) and eliminate the current from Eq. (9) to obtain an effective diffusion equation for the density of motile particles, given by

$$\partial_t \rho_G(\mathbf{r}, t) = -\beta \rho_R \rho_G + \mu \rho_R + \nabla \cdot [\mathcal{D}(\rho_G) \nabla \rho_G] - \kappa \nabla^4 \rho_G, \quad (12)$$

where

$$\mathcal{D}(\rho_G) = \frac{v(\rho_G)}{2\lambda_{eff}(\rho_R)} [v(\rho_G) + \rho_G v'(\rho_G)], \quad (13)$$

with the prime denoting a derivative with respect to density, is an effective diffusivity that incorporates the effects of crowding due to motility [33–35]. Note that \mathcal{D} can change sign, signaling the spinodal instability associated with MIPS. We therefore expect that at high enough density the structural properties of the system will be controlled by the interplay of MIPS physics and the exchange of internal motility state regulated by collisions and reawakening.

We now examine the linear stability of the two homogeneous steady states to spatially varying fluctuations. We write $\rho_{G,R} = \rho_{G,R}^0 + \delta \rho_{G,R}$, where $\rho_{G,R}^0$ are the homogeneous fixed points, and expand to linear order in the fluctuations. Working in Fourier space, we let $\delta \rho_{G,R} = \sum_{\mathbf{q}} e^{i\mathbf{q}\cdot\mathbf{r}} \hat{\rho}_{G,R}(\mathbf{q})$. The linearized equations for the Fourier amplitudes are then given by

$$\partial_t \hat{\rho}_R = (\beta \rho_G^0 - \mu) \hat{\rho}_R + \beta \rho_R^0 \hat{\rho}_G, \quad (14)$$

$$\partial_t \hat{\rho}_G = (\mu - \beta \rho_G^0) \hat{\rho}_R - (\beta \rho_R^0 + \mathcal{D}(\rho_G^0) q^2 + \kappa q^4) \hat{\rho}_G. \quad (15)$$

a. Stability of motile state. When reawakening is faster than collisions ($\mu > \mu_c = \beta\rho_0$), the homogeneous state is the absorbing state where all particles are motile, i.e., $\rho_G^0 = \rho_0$ and $\rho_R^0 = 0$. In this case Eqs. (19) and (20) are decoupled. Letting $\hat{\rho}_{G,R}(t) \sim e^{i\omega t} \hat{\rho}_{G,R}^0$, the dispersion relations of the relaxation rates are

$$i\omega_R = -\mu + \beta\rho_0 \quad (16)$$

$$i\omega_G = -(\mathcal{D}_0 q^2 + \kappa q^4), \quad (17)$$

where

$$\mathcal{D}(\rho_0) = \frac{v_0^2}{2\lambda} \left(1 - \frac{\rho_0}{\rho^*}\right) \left(1 - 2\frac{\rho_0}{\rho^*}\right) \quad (18)$$

becomes negative at $\rho_0 = \rho^*/2$. Fluctuations in the density of non-motile particles always decay. On the other hand, fluctuations in the density of motile particles grow when $\mathcal{D}(\rho_0) < 0$. The motile particle aggregate and undergo MIPS for $\rho_0 > \rho^*/2$. Therefore if $\rho^* < \mu/\beta$ the motile state will be homogeneous for $\rho_0 < \rho^*/2$ and will undergo MIPS for $\rho^*/2 < \rho_0 < \mu/\beta$.

b. Stability of mixed state. When collisions dominate over reawakening ($\mu < \mu_c = \beta\rho_0$), the final state always contains a fraction of non-motile particles, with $\rho_G^0 = \mu/\beta$ and $\rho_R^0 = \rho_0 - \mu/\beta$. In this case the linearized equations become

$$\partial_t \hat{\rho}_R = (\beta\rho_0 - \mu) \hat{\rho}_G, \quad (19)$$

$$\partial_t \hat{\rho}_G = -(\beta\rho_0 - \mu + \mathcal{D}(\rho_G^0) q^2 + \kappa q^4) \hat{\rho}_G. \quad (20)$$

Fluctuations in the density of non-motile particles are slaved to those in the density of motiles ones, whose decay is controlled by the rate

$$i\omega_m = -(\beta\rho_0 - \mu + \mathcal{D}(\rho_G^0) q^2 + \kappa q^4), \quad (21)$$

with

$$\mathcal{D}(\rho_G^0) = \frac{v_0^2}{2(\lambda + \mu)} \left(1 - \frac{\mu}{\beta\rho^*}\right) \left(1 - 2\frac{\mu}{\beta\rho^*}\right). \quad (22)$$

The mixed homogeneous state is then unstable if the following conditions are satisfied

$$\mathcal{D}(\rho_G^0) < 0 \quad \text{and} \quad |\mathcal{D}(\rho_G^0)| > \sqrt{4\kappa(\beta\rho_0 - \mu)}. \quad (23)$$

The first condition is satisfied for $\mu/\beta > \rho^*/2$, which provides a necessary, but not sufficient condition for the instability. At the onset of instability only one mode is unstable, with wavevector

$$q_0 = (|\mathcal{D}(\rho_G^0)|/2\kappa)^{1/2} \sim (\mu/\beta - \rho^*/2)^{1/2}, \quad (24)$$

which sets the length scale of the spatial pattern.

In this regime fluctuations in the density of non-motile particles are slaved to those in the density of motile ones. As a result, both go unstable for $\rho_0 > \rho^*/2$ above a critical value $\mu_m(\rho_0)$ of the reawakening rate given by the solution of Eqs. (23). As a result, the system shows regions that are essentially void of particles in a well mixed background. This is seen in our numerical simulations at high density. Although the numerics do not seem to show the emergence of patterns at a characteristic length scale, the size of the voids does increase with increasing μ as seen in the third and fourth column of Fig. 1, consistent with Eq.(24).

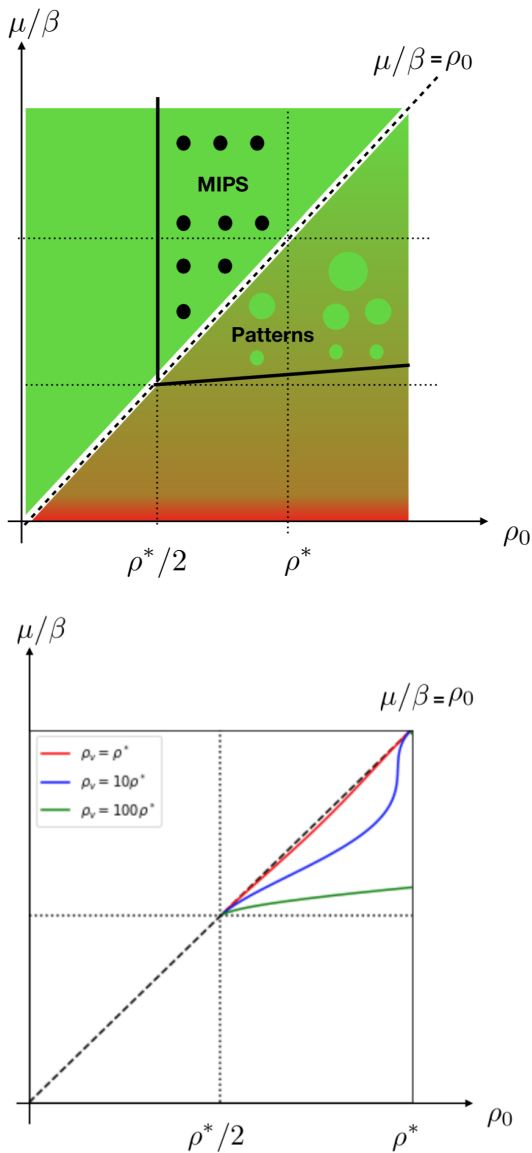


FIG. 10: Top: phase diagram obtained from linear stability analysis of the continuum model. The motile steady state for $\mu/\beta > \rho_0$ is homogeneous for $\rho_0 < \rho^*/2$, while the motile (G) particles undergo MIPS for $\rho_0 > \rho^*/2$. In the mixed state for $\mu/\beta < \rho_0$ motile and non-motile particles are uniformly mixed for values of the reawakening frequency below the critical line determined by the solution of Eq.(23) and shown in the figure for $\rho_v = v_0^4/(16\lambda^2\kappa\beta)$. Above this line, fluctuations in the density of both motile and nonmotile particles are unstable, resulting in spatial patterns. Bottom: stability boundaries in the mixed state for different values of the characteristic density $\rho_v = \rho^*, 10\rho^*, 100\rho^*$ (with μ/β , and ρ_0 also measured in units of ρ^*). For simplicity we have neglected the renormalization of λ .

V. CONCLUSIONS

We have used numerics and mean-field theory to study a model of active particles carrying a Boolean variable

coupled to their motility. When the motility state is exchanged irreversibly according to AND and OR logic rules, the system always evolves towards an absorbing state where all particles are motile (OR) or non-motile (AND), as shown in earlier work [28]. The coupling between motility and the spreading of information affects this irreversible dynamics, as evidenced by the asymmetry of the relaxation. OR particles relax faster than AND particles, as shown in Fig. 4, because their collisional reaction rate is enhanced by activity, consistent with a simple mean-field estimate. The key role of motility is also highlighted by examining a model where the internal state that evolves according to Boolean rules is simply the particles' color, while the particles remain motile at all times. In this case the relaxation of AND and OR particles is identical.

When AND particles are allowed to reacquire their motility at a rate μ , we find both absorbing and active steady states controlled by the interplay of collision and reawakening rates. For μ above a critical value μ_c the system evolves towards an absorbing state where all particles are motile. For $0 < \mu < \mu_c$ the system evolves towards an active state with finite fractions of motile and non-motile particles, recovering the absorbing state of non-motile particles only at $\mu = 0$. The value of μ_c is controlled by the total packing fraction and the collision rate. The steady state exhibits a rich spatial structure, with motility-induced phase separation of motile particles in the high density motile absorbing state and aggregation of non-motile particles or void formation in the active mixed state. Some of this behavior is reproduced by a mean-field model that incorporate suppression of motility due to crowding as in models of MIPS.

We have focused our attention on pattern formation in the mixed state. We showed that different types of aggregates have been developed by logic interaction. At intermediate densities, the formation of aggregates is driven by the reaction-diffusion process that leads to the spreading of a cluster of nonmotile particles. At high densities, the phase separation is driven by motility. In both cases, the non-equilibrium structural phase transition between homogeneous and phase-separated state shows features of a first-order phase transition that is signaled by a negative peak of the Binder cumulant g_4 . We leave the detailed study of the absorbing state phase transition for future work.

The simple model studied here provides a step towards understanding the role of motility in information spreading. Specifically, the model of AND particles with reawakening is analog to SIS models of epidemic spreading, but, in contrast to most existing studies, where infection is spread on a static network, here we examine the case where the infection is spread by *motile* agent and demonstrate that motility affects both the dynamics and the structure of the final state. The interplay of information spreading and motility is also relevant to pattern formation in bacterial colonies containing phenotypes with different motility, such as single- and multi-

flagellated *Pseudomonas aeruginosa*[48] or *B. Subtilis*, where a crossover from fractal to compact bacterial aggregates has been observed [49], as well as to understanding of biofilm formation.

Acknowledgements

MCM was supported by the US National Science Foundation through award DMR-1609208. MP acknowledges funding from Regione Lazio, Grant Prot. n. 85-2017-15257 ("Progetti di Gruppi di Ricerca - Legge 13/2008 - art. 4"). This work was also supported by the Joint Laboratory on "Advanced and Innovative Materials", ADIN-MAT, WIS Sapienza (MP).

Appendix A: Renormalization of tumbling rate by interactions

In this Appendix we show that the exchange of the particle state through collisions yields a renormalization of the tumbling rate. For simplicity, we carry out the calculation for the case of Active Brownian Particles (ABP) instead of Run-and-Tumble Particles (RTP). For ABP interacting with AND logic rules, we show that the rotational noise D_r is renormalized by interactions to the value $D_r^{eff} = D_r = \beta \rho_R$, where β is the collision rate per unit density. Correspondingly, for RTP with AND interaction rule the effective tumbling rate is $\lambda_{eff} = \lambda + \beta \rho_R$. We also provide an estimate of the parameter β .

We consider N ABP at positions \mathbf{x}_n interacting with purely repulsive interactions with an internal state described by $s_n = \pm 1$ ($s_n = 1$ motile, $s_n = -1$ non-motile) and orientation $\hat{\mathbf{u}}_n$. The internal state variable s_n is related to the state variable σ used in numerical simulations through $\sigma_n = \frac{s_n + 1}{2}$. The dynamics is described by coupled Langevin-like equations, given by

$$\dot{\mathbf{x}}_n = \frac{(1 + s_n)}{2} v_0 \hat{\mathbf{u}}_n, \quad (\text{A1})$$

$$\dot{s}_n = -\beta \sum_{m \neq n} (s_n + 1) \delta(s_n + s_m) \delta(\mathbf{x}_n - \mathbf{x}_m), \quad (\text{A2})$$

$$\dot{\hat{\mathbf{u}}}_n = \frac{(1 + s_n)}{2} \hat{\mathbf{z}} \times \hat{\mathbf{u}}_n \sqrt{2D_r} \eta_n(t). \quad (\text{A3})$$

The right hand side of Eq.(A1) describes self-propulsion, which is zero if $s_n = -1$ (non-motile). The effect of interactions is only included in Eq.(A2), where interactions with non-motile agent change the motility state of the particle. It is not included in the translational dynamics that has been considered elsewhere [47]. The factor $s_n + 1$ in Eq.(A2) accounts for the sign of the derivative, which must be negative when switching from $+1$ to -1 . Finally, Eq.(A3) describes the dynamics of the orientation $\hat{\mathbf{u}}_n$, with D_r the rotational diffusivity and $\eta_n(t)$ Gaussian white noise with unit variance.

The parameter β can be estimated as $\beta = (\rho_0 \tau_c)^{-1}$, where ρ_0 is the mean density of particles and τ_c the mean free time between collisions. For a system of particles traveling with mean speed $\langle v \rangle$ and density ρ_0 , then $\tau_c = (\rho \langle v \rangle \sigma_c)^{-1}$, where σ_c is the collision cross section, determined by the form of the repulsive potential. The mean-free path is then $\ell_c = \langle v \rangle \tau_c$.

At high density, the mean free path is smaller than the persistence length, $\ell_p = v_0/D_r$, or $\ell_c < \ell_p$, corresponding to $\rho_0 > D_r/(v_0 \sigma)$, particles travel ballistically between collisions, hence $\langle v \rangle = v_0$. This gives $\beta \sim v_0 \sigma_c \sim v_0 \rho_0^{-1/2}$ where in the last approximate equality we have assumed that at high density $\sigma_c \sim \rho_0^{-1/2}$.

At low density, $\ell_c > \ell_p$ and particles travel diffusively with diffusion coefficient $D_0 = \frac{v_0^2}{2D_r}$. This gives $\beta \sim v_0 \sigma_c$, independent of density. In both limits our estimates are consistent with the results presented in [28].

To derive continuum equations we focus on the dynamics of the one-particle probability density [50], given by

$$c(\mathbf{r}, \hat{\mathbf{u}}, s, t) = \langle \delta(\mathbf{r} - \mathbf{x}(t)) \delta(\hat{\mathbf{u}} - \hat{\mathbf{u}}(t)) \delta(s - s(t)) \rangle \quad (\text{A4})$$

that measures the probability of finding a particle with position \mathbf{r} , orientation $\hat{\mathbf{u}}$ and internal state s at time t .

The dynamics of the probability density is governed by a Smoluchowski equation that can be derived by standard procedure from the Langevin equations Eq.(A1) - Eq.(A3), [51] Due to binary collisions, the equation for c couples to the two particle distribution function $c_2(\mathbf{x}, \hat{\mathbf{u}}, s, t; \mathbf{x}', \hat{\mathbf{u}}', s', t)$. Using a Boltzmann-type of approximation [51], we treat the two microscopic densities as uncorrelated and let $c_2(\mathbf{x}, \hat{\mathbf{u}}, s, t; \mathbf{x}', \hat{\mathbf{u}}', s', t) \approx c(\mathbf{x}, \hat{\mathbf{u}}, s, t) c(\mathbf{x}', \hat{\mathbf{u}}', s', t)$, with the result

$$\begin{aligned} \partial_t c = & -\frac{1+s}{2} \nabla_x (v_0 \hat{\mathbf{u}} c) - \frac{(1+s)^2}{4} D_r \mathcal{R} \cdot \mathcal{R} c \\ & + \partial_s \left(\beta(s+1) c(\mathbf{r}, \hat{\mathbf{u}}, s, t) \int d\hat{\mathbf{u}}' c(\mathbf{r}, \hat{\mathbf{u}}', -s, t) \right), \end{aligned} \quad (\text{A5})$$

where $\mathcal{R} = \hat{\mathbf{u}} \times \frac{\partial}{\partial \hat{\mathbf{u}}}$ is a rotation operator.

We then write the total concentration as the sum of the concentrations of motile and non-motile particles $c_{G,R} = \sum_s \frac{(1 \pm s)}{2} c \approx \int_s \frac{(1 \pm s)}{2} c$ and introduce densities $\rho_{G,R} = \int d\hat{\mathbf{u}} c_{G,R}$ and the polar vector $\mathbf{J} = v_0 \int d\hat{\mathbf{u}} \hat{\mathbf{u}} c_G$. We carry out the integrals in s using Leibnitz rule for functions defined on compact spaces, where $\int ds f(s) \partial_s g(s) = - \int ds g(s) \partial_s [f(s)]$. Thus we obtain

$$\partial_t c_G = -\nabla_{\mathbf{r}} (v_0 \hat{\mathbf{u}} c_G) - D_r \mathcal{R} \cdot \mathcal{R} c_G \quad (\text{A6})$$

$$\begin{aligned} & -\beta c_G(\mathbf{r}, \hat{\mathbf{u}}, t) \rho_R(\mathbf{r}, t), \\ \partial_t c_R = & \beta c_G(\mathbf{r}, \hat{\mathbf{u}}, t) \rho_R(\mathbf{r}, t). \end{aligned} \quad (\text{A7})$$

Finally, integrating Eq.(A6) and Eq.(A7) over $\hat{\mathbf{u}}$, we

obtain Eq.(A6) and Eq.(A7), with the result

$$\partial_t \rho_G = -\nabla_{\mathbf{r}} \mathbf{J} - \beta \rho_G \rho_R, \quad (\text{A8})$$

$$\partial_t \rho_R = \beta \rho_G \rho_R, \quad (\text{A9})$$

$$\partial_t \mathbf{J} = -\frac{1}{2} \nabla_{\mathbf{r}} (v_0^2 \rho_G) - (D_r + \beta \rho_R) \mathbf{J}. \quad (\text{A10})$$

-
- [1] M. C. Marchetti *et al.*, *Rev. Mod. Phys.*, 2013, **85**, 1143.
[2] M. E. Cates, *Rep. Prog. Phys.*, 2012, **75**, 042601.
[3] S. Ramaswamy, *Annual Review of Condensed Matter Physics*, 2010, **1**, 323–345.
[4] C. Bechinger, R. Di Leonardo, H. Löwen, C. Reichhardt, G. Volpe and G. Volpe, *Rev. Mod. Phys.*, 2016, **88**, 045006.
[5] B. Smeets, R. Alert, J. Pešek, I. Pagonabarraga, H. Ramon and R. Vincent, *Proceedings of the National Academy of Sciences*, 2016, **113**, 14621–14626.
[6] D. Levis, I. Pagonabarraga and B. Liebchen, *Phys. Rev. Research*, 2019, **1**, 023026.
[7] D. Levis, I. Pagonabarraga and A. Díaz-Guilera, *Phys. Rev. X*, 2017, **7**, 011028.
[8] L. G. Nava, R. Großmann and F. Peruani, *Phys. Rev. E*, 2018, **97**, 042604.
[9] G. J. SIBONA, F. PERUANI and G. R. TERRANOVA, in *BIOMAT 2011*, World Scientific, 2012, pp. 241–252.
[10] F. Peruani and G. J. Sibona, *Phys. Rev. Lett.*, 2008, **100**, 168103.
[11] F. Peruani and G. J. Sibona, *Soft matter*, 2019, **15**, 497–503.
[12] L. Keller and M. G. Surette, *Nature Reviews Microbiology*, 2006, **4**, 249.
[13] M. E. Hibbing, C. Fuqua, M. R. Parsek and S. B. Peterson, *Nature Reviews Microbiology*, 2010, **8**, 15.
[14] G. H. Wadhams and J. P. Armitage, *Nature reviews Molecular cell biology*, 2004, **5**, 1024.
[15] P. J. Van Haastert and P. N. Devreotes, *Nature reviews Molecular cell biology*, 2004, **5**, 626.
[16] J. Agudo-Canalejo and R. Golestanian, *Phys. Rev. Lett.*, 2019, **123**, 018101.
[17] J. S. Bois, F. Julicher and S. W. Grill, *Phys. Rev. Lett.*, 2011, **106**,.
[18] B. Libchen, M. E. Cates and D. Marenduzzo, *SoftMatter*, 2016, **12**, 7259–7264.
[19] J. R. Gomez-Solano *et al.*, *Sci. Rep.*, 2017, **7**, 14891.
[20] T. Baurle *et al.*, *Nature Comm.*, 2018, **9**, 3232.
[21] G. Frangipane, D. Dell’Arciprete, S. Petracchini, C. Maggi, F. Saglimbeni, S. Bianchi, G. Viznyiczai, M. L. Bernardini and R. Di Leonardo, *Elife*, 2018, **7**, e36608.
[22] J. Arlt, V. A. Martinez, A. Dawson, T. Pilizota and W. C. Poon, *Nature communications*, 2018, **9**, 768.
[23] S. Muinos-Landin *et al.*, <https://arxiv.org/abs/1803.06425>, 2018.
[24] M. Rubenstein, A. Cornejo and R. Nagpal, *Science*, 2014, **345**, 795–799.
[25] E. Agliari, R. Burioni, D. Cassi and F. M. Neri, *Physical Review E*, 2006, **73**, 046138.
[26] N. Ferguson, *Nature*, 2007, **446**, 733.
[27] R. Pastor-Satorras, C. Castellano, P. Van Mieghem and A. Vespignani, *Rev. Mod. Phys.*, 2015, **87**, 925–979.
[28] M. Paoluzzi, M. Leoni and M. C. Marchetti, *Phys. Rev. E*, 2018, **95**, 052603.
[29] J. D. Murray, *Mathematical Biology*, Springer Verlag (Berlin Heidelberg), 1989.
[30] G. Ódor, *Rev. Mod. Phys.*, 2004, **76**, 663–724.
[31] H. Hinrichsen, *Advances in physics*, 2000, **49**, 815–958.
[32] J. Tailleur and M. E. Cates, *Phys. Rev. Lett.*, 2008, **100**, 218103.
[33] Y. Fily and M. C. Marchetti, *Phys. Rev. Lett.*, 2012, **108**, 235702.
[34] M. E. Cates and J. Tailleur, *Annu. Rev. Condens. Matter Phys.*, 2015, **6**, 219–244.
[35] Y. Fily, S. Henkes and M. C. Marchetti, *Soft matter*, 2014, **10**, 2132–2140.
[36] A. Patch, D. M. Sussman, D. Yllanes and M. C. Marchetti, *Soft matter*, 2018, **14**, 7435–7445.
[37] M. J. Keeling and P. Rohani, *Modelling infectious diseases in humans and animals*, Princeton University Press, 2008.
[38] C. Castellano, S. Fortunato and V. Loreto, *Rev. Mod. Phys.*, 2009, **81**, 591.
[39] A. V. Goltsev, S. N. Dorogovtsev, J. G. Oliveira and J. F. F. Mendes, *Phys. Rev. Lett.*, 2012, **109**, 128702.
[40] S. Riley, *Science*, 2007, **316**, 1298–1301.
[41] M. Paoluzzi, R. Di Leonardo and L. Angelani, *Journal of Physics: Condensed Matter*, 2013, **25**, 415102.
[42] M. Paoluzzi, R. Di Leonardo and L. Angelani, *Journal of Physics: Condensed Matter*, 2014, **26**, 375101.
[43] K. Binder, *Zeitschrift für Physik B Condensed Matter*, 1981, **43**, 119–140.
[44] M. Rovere, D. Hermann and K. Binder, *EPL (Europhysics Letters)*, 1988, **6**, 585.
[45] M. Rovere, *Journal of Physics: Condensed Matter*, 1993, **5**, B193.
[46] K. Binder, *Reports on Progress in Physics*, 1997, **60**, 487.
[47] R. Wittkowski *et al.*, *New J. Phys.*, 2017, **19**, 105003.
[48] M. Deforet, D. Van Ditmarsch, C. Carmona-Fontaine and J. B. Xavier, *Soft matter*, 2014, **10**, 2405–2413.
[49] M. Matsushita, F. Hiramatsu, N. Kobayashi, T. Ozawa, Y. Yamazaki and T. Matsuyama, *Biofilms*, 2004, **1**, 305–317.
[50] T. B. Liverpool and M. C. Marchetti, *Phys. Rev. Lett.*, 2003, **90**, 138102.
[51] R. Zwanzig, *Nonequilibrium Statistical Mechanics*, Oxford University Press, 2001.